Research Article | Vol. 8, No. 12 | 1 Dec 2017 | BIOMEDICAL OPTICS EXPRESS 5374
Biomedical Optics EXPRESS

Correlative imaging of biological tissues with apertureless scanning near-field optical microscopy and confocal laser scanning microscopy

STEFAN G. STANCIU,* DENIS E. TRANCA, RADU HRISTU, AND GEORGE A. STANCIU

Center for Microscopy-Microanalysis and Information Processing, University Politehnica of Bucharest, Bucharest, 060042, Romania
**stefan.stanciu@cmmip-upb.org*

Abstract: Apertureless scanning near-field optical microscopy (ASNOM) has attracted considerable interest over the past years as a result of its valuable contrast mechanisms and capabilities for optical resolutions in the nanoscale range. However, at this moment the intersections between ASNOM and the realm of bioimaging are scarce, mainly due to data interpretation difficulties linked to the limited body of work performed so far in this field and hence the reduced volume of supporting information. We propose an imaging approach that holds significant potential for alleviating this issue, consisting of correlative imaging of biological specimens using a multimodal system that incorporates ASNOM and confocal laser scanning microscopy (CLSM), which allows placing near-field data into a well understood context of anatomical relevance. We demonstrate this approach on zebrafish retinal tissue. The proposed method holds important implications for the in-depth understanding of biological items through the prism of ASNOM and CLSM data complementarity.

OCIS codes: (180.4243) Near-field microscopy; (180.1790) Confocal microscopy; (170.0110) Imaging systems; (170.6935) Tissue characterization.

References and links

1. W. R. Zipfel, R. M. Williams, R. Christie, A. Y. Nikitin, B. T. Hyman, and W. W. Webb, "Live tissue intrinsic emission microscopy using multiphoton-excited native fluorescence and second harmonic generation," Proc. Natl. Acad. Sci. U.S.A. **100**(12), 7075–7080 (2003).
2. J. P. Pezacki, J. A. Blake, D. C. Danielson, D. C. Kennedy, R. K. Lyn, and R. Singaravelu, "Chemical contrast for imaging living systems: molecular vibrations drive CARS microscopy," Nat. Chem. Biol. **7**(3), 137–145 (2011).
3. K. König, "Clinical multiphoton tomography," J. Biophotonics **1**(1), 13–23 (2008).
4. E. D. Hawkins, D. Duarte, O. Akinduro, R. A. Khorshed, D. Passaro, M. Nowicka, L. Straszkowski, M. K. Scott, S. Rothery, N. Ruivo, K. Foster, M. Waibel, R. W. Johnstone, S. J. Harrison, D. A. Westerman, H. Quach, J. Gribben, M. D. Robinson, L. E. Purton, D. Bonnet, and C. Lo Celso, "T-cell acute leukaemia exhibits dynamic interactions with bone marrow microenvironments," Nature **538**(7626), 518–522 (2016).
5. S. Nori, F. Rius-Díaz, J. Cuevas, M. Goldgeier, P. Jaen, A. Torres, and S. González, "Sensitivity and specificity of reflectance-mode confocal microscopy for in vivo diagnosis of basal cell carcinoma: a multicenter study," J. Am. Acad. Dermatol. **51**(6), 923–930 (2004).
6. Z. Wu, T. Rademakers, F. Kiessling, M. Vogt, E. Westein, C. Weber, R. T. A. Megens, and M. van Zandvoort, "Multi-Photon Microscopy in Cardiovascular Research," Methods **130**, 79–89 (2017).
7. M. Meyer-Luehmann, T. L. Spires-Jones, C. Prada, M. Garcia-Alloza, A. de Calignon, A. Rozkalne, J. Koenigsknecht-Talboo, D. M. Holtzman, B. J. Bacskai, and B. T. Hyman, "Rapid appearance and local toxicity of amyloid-β plaques in a mouse model of Alzheimer's disease," Nature **451**(7179), 720–724 (2008).
8. C. Cremer and U. Birk, "Perspectives in super-resolved fluorescence microscopy: What comes next?" Front. Phys. **4**, 11 (2016).
9. S. W. Hell, S. J. Sahl, M. Bates, X. Zhuang, R. Heintzmann, M. J. Booth, J. Bewersdorf, G. Shtengel, H. Hess, and P. Tinnefeld, "The 2015 super-resolution microscopy roadmap," J.Phys. D. **48**(44), 443001 (2015).
10. P. Wang, M. N. Slipchenko, J. Mitchell, C. Yang, E. O. Potma, X. Xu, and J.-X. Cheng, "Far-field imaging of non-fluorescent species with subdiffraction resolution," Nat. Photonics **7**(6), 449–453 (2013).

#307441 https://doi.org/10.1364/BOE.8.005374
Journal © 2017 Received 19 Sep 2017; revised 1 Nov 2017; accepted 1 Nov 2017; published 7 Nov 2017

Biomedical Optics EXPRESS

11. D. Nowak, W. Morrison, H. K. Wickramasinghe, J. Jahng, E. Potma, L. Wan, R. Ruiz, T. R. Albrecht, K. Schmidt, J. Frommer, D. P. Sanders, and S. Park, "Nanoscale chemical imaging by photoinduced force microscopy," Sci. Adv. **2**(3), e1501571 (2016).
12. F. Keilmann and R. Hillenbrand, "Near-field microscopy by elastic light scattering from a tip," Philos. Trans. A Math. Phys. Eng. Sci. **362**(1817), 787–805 (2004).
13. A. J. Huber, A. Ziegler, T. Köck, and R. Hillenbrand, "Infrared nanoscopy of strained semiconductors," Nat. Nanotechnol. **4**(3), 153–157 (2009).
14. S. G. Stanciu, D. E. Tranca, C. Ruggiero, G. A. Stanciu, E. Dellacasa, A. Antipov, R. Hristu, and L. Pastorino, "Combined far-field, near-field and topographic imaging of nano-engineered polyelectrolyte capsules," Mater. Lett. **183**, 105–108 (2016).
15. D. E. Tranca, S. G. Stanciu, R. Hristu, C. Stoichita, S. A. Tofail, and G. A. Stanciu, "High-resolution quantitative determination of dielectric function by using scattering scanning near-field optical microscopy," Sci. Rep. **5**, 11876 (2015).
16. A. Cvitkovic, N. Ocelic, and R. Hillenbrand, "Material-specific infrared recognition of single sub-10 nm particles by substrate-enhanced scattering-type near-field microscopy," Nano Lett. **7**(10), 3177–3181 (2007).
17. J. M. Stiegler, R. Tena-Zaera, O. Idigoras, A. Chuvilin, and R. Hillenbrand, "Correlative infrared-electron nanoscopy reveals the local structure-conductivity relationship in zinc oxide nanowires," Nat. Commun. **3**, 1131 (2012).
18. J. M. Stiegler, A. J. Huber, S. L. Diedenhofen, J. G. Rivas, R. E. Algra, E. P. Bakkers, and R. Hillenbrand, "Nanoscale free-carrier profiling of individual semiconductor nanowires by infrared near-field nanoscopy," Nano Lett. **10**(4), 1387–1392 (2010).
19. D. E. Tranca, E. Sánchez-Ortiga, G. Saavedra, M. Martínez-Corral, S. A. Tofail, S. G. Stanciu, R. Hristu, and G. A. Stanciu, "Mapping electron-beam-injected trapped charge with scattering scanning near-field optical microscopy," Opt. Lett. **41**(5), 1046–1049 (2016).
20. R. Hillenbrand, B. Knoll, and F. Keilmann, "Pure optical contrast in scattering-type scanning near-field microscopy," J. Microsc. **202**(Pt 1), 77–83 (2001).
21. T. Taubner, R. Hillenbrand, and F. Keilmann, "Performance of visible and mid-infrared scattering-type near-field optical microscopes," J. Microsc. **210**(Pt 3), 311–314 (2003).
22. N. Ocelic, A. Huber, and R. Hillenbrand, "Pseudoheterodyne detection for background-free near-field spectroscopy," Appl. Phys. Lett. **89**(10), 101124 (2006).
23. D. E. Tranca, C. Stoichita, R. Hristu, S. G. Stanciu, and G. A. Stanciu, "A study on the image contrast of pseudo-heterodyned scattering scanning near-field optical microscopy," Opt. Express **22**(2), 1687–1696 (2014).
24. A. V. Zayats and V. Sandoghdar, "Apertureless near-field optical microscopy via local second-harmonic generation," J. Microsc. **202**(Pt 1), 94–99 (2001).
25. T. Yang, G. A. Lessard, and S. R. Quake, "An apertureless near-field microscope for fluorescence imaging," Appl. Phys. Lett. **76**(3), 378–380 (2000).
26. O. Schulz, Z. Zhao, A. Ward, M. Koenig, F. Koberling, Y. Liu, J. Enderlein, H. Yan, and R. Ros, "Tip induced fluorescence quenching for nanometer optical and topographical resolution," Opt. Nanoscopy **2**, 1 (2013).
27. J. M. Mateos, B. Guhl, J. Doehner, G. Barmettler, A. Kaech, and U. Ziegler, "Topographic contrast of ultrathin cryo-sections for correlative super-resolution light and electron microscopy," Sci. Rep. **6**, 34062 (2016).
28. J. M. Mateos, G. Barmettler, J. Doehner, I. O. Naharros, B. Guhl, S. C. F. Neuhauss, A. Kaech, R. Bachmann-Gagescu, and U. Ziegler, "Correlative Super-resolution and Electron Microscopy to Resolve Protein Localization in Zebrafish Retina," J. Vis. Exp. in production (2017).
29. J. Wan and D. Goldman, "Retina regeneration in zebrafish," Curr. Opin. Genet. Dev. **40**, 41–47 (2016).
30. C. N. Keilhauer and F. C. Delori, "Near-infrared autofluorescence imaging of the fundus: visualization of ocular melanin," Invest. Ophthalmol. Vis. Sci. **47**(8), 3556–3564 (2006).
31. D. N. Hu, J. D. Simon, and T. Sarna, "Role of ocular melanin in ophthalmic physiology and pathology," Photochem. Photobiol. **84**(3), 639–644 (2008).
32. T. Sarna, "Properties and function of the ocular melanin-a photobiophysical view," J. Photochem. Photobiol. B **12**(3), 215–258 (1992).
33. D. E. Tranca, S. G. Stanciu, R. Hristu, B.M. Witgen, and G. A. Stanciu, "Nanoscale mapping of refractive index by using scattering-type Scanning Near-Field Optical Microscopy," Nanomed. Nanotech. Biol. Med. in press (2017).
34. D. K. Sardar, M. L. Mayo, and R. D. Glickman, "Optical characterization of melanin," J. Biomed. Opt. **6**(4), 404–411 (2001).
35. M. Brehm, T. Taubner, R. Hillenbrand, and F. Keilmann, "Infrared spectroscopic mapping of single nanoparticles and viruses at nanoscale resolution," Nano Lett. **6**(7), 1307–1310 (2006).
36. T. Taubner, F. Keilmann, and R. Hillenbrand, "Nanoscale-resolved subsurface imaging by scattering-type near-field optical microscopy," Opt. Express **13**(22), 8893–8899 (2005).
37. H. Wang, L. Wang, D. S. Jakob, and X. G. Xu, "Mapping three-dimensional near-field responses with reconstruction scattering-type scanning near-field optical microscopy," AIP Adv. **7**, 055118 (2017).
38. A. P. Engelhardt, B. Hauer, and T. Taubner, "Visibility of weak contrasts in subsurface scattering near-field microscopy," Ultramicroscopy **126**, 40–43 (2013).
39. E. L. Moal, E. Fort, S. Lévêque-Fort, F. P. Cordelières, M.-P. Fontaine-Aupart, and C. Ricolleau, "Enhanced fluorescence cell imaging with metal-coated slides," Biophys. J. **92**(6), 2150–2161 (2007).

Biomedical Optics EXPRESS

40. U. Kellner, S. Kellner, B. H. Weber, B. Fiebig, S. Weinitz, and K. Ruether, "Lipofuscin- and melanin-related fundus autofluorescence visualize different retinal pigment epithelial alterations in patients with retinitis pigmentosa," Eye (Lond.) **23**(6), 1349–1359 (2009).

1. Introduction

The field of Laser Scanning Microscopy (LSM) is greatly responsible for our current unprecedented possibilities for imaging biological species. Techniques such as Confocal Laser Scanning Microscopy (CLSM), Multiphoton Microscopy (MPM) or Coherent Anti-Stokes Raman Scattering Microscopy (CARS) represent nowadays essential tools for studying organelles, cells and tissues (or proteins and antibodies). They offer crucial advantages for resolving significant physiological and pathological aspects [1, 2] that are important for understanding, diagnosing, and treating severe maladies such as cancers [3–5], cardiovascular [6] or neurodegenerative diseases [7]. The lateral resolution that can be achieved by using such (now classical) LSM techniques is limited by diffraction to ~200nm, depending on the wavelength being used. This resolution limit impedes an exact understanding of many fundamental structures and processes at cellular and sub-cellular levels, higher resolution being necessary for elucidating aspects that are still not well understood. In response to the need for higher resolution, the field of science dealing with optical imaging beyond the diffraction barrier, namely Super-Resolution Microscopy (SRM), has become one of the hot topics of the imaging community (developers and users). Fluorescence based SRM techniques such as Stimulated Emission Depletion Microscopy (STED), Reversible Saturable Optical Fluorescence Transitions Microscopy (RESOLFT), Structured Illumination Microscopy (SIM), Fluorescence Photoactivation Localization Microscopy (f-PALM) or Stochastical Optical Reconstruction Microscopy (STORM), succeed in overcoming the resolution limits imposed by diffraction, offering typical resolutions in the range of 20-100nm. The importance of these (still "young") techniques was recently highlighted by the 2014 Nobel Prize in Chemistry that was awarded jointly to Eric Betzig, Stefan W. Hell and William E. Moerner *"for the development of super-resolved fluorescence microscopy"*. Although enormously useful, fluorescence based SRM techniques face a series of limitations, as they are not chemically sensitive and require fluorescent probes, which often times add artifacts to the investigated samples. In the same time fluorescent labeling can influence the metabolic processes in the cells that are imaged, and lead to cytotoxicity and phototoxicity [8, 9]. Such limitations have motivated scientists to search in parallel alternative ways of overcoming the resolution limits imposed by diffraction, in the form of imaging techniques that do not require markers. Among these, techniques such as Apertureless Scanning Near-Field Optical microscopy (ASNOM), pump and probe nanoscopy based on saturated transient absorption [10] or photoinduced force microscopy [11] hold significant potential for advancing beyond the state-of-the-art the current understanding on the structural, chemical and optical features of biological samples, materials or devices. When compared to fluorescence based ones, they can provide complementary or equivalent information based on complex contrast mechanisms that exploit different physical underpinnings.

In scattering-type Scanning Near-Field Optical Microscopy (s-SNOM) [12], the ASNOM variant employed in our experiment, the interaction between a laser beam and a sharp tip is exploited for optically probing an investigated sample at nanoscale resolutions. Upon excitation, the tip converts the illumination radiation into a highly localized and enhanced near-field at the tip apex. The optical interaction between this enhanced near-field and the sample volume underneath modifies both the amplitude and the phase of the scattered excitation light, depending on the local dielectric properties of the sample [12]. Interferometric detection of the backscattered light yields nanoscale-resolved amplitude and phase images, revealing besides local structural properties [13, 14], also additional aspects such as material composition [15, 16], free-carrier concentration [17, 18] or surface charge domains [19]. The resolution achievable with s-SNOM is connected to the tip's radius of

Biomedical Optics EXPRESS

curvature, falling well under 40 nm [12, 20], and is independent of the illumination wavelength [21].

ASNOM holds significant potential for resolving cellular and tissular features of physiological and pathological relevance at optical resolutions lying in the nanoscale range, but due to the limited body of work performed so far in the ASNOM bioimaging area, and hence the reduced volume of supporting information, the interpretation of near-field data sets collected using ASNOM variants usually turns out to be cumbersome. This problem can be alleviated by collecting supporting information on the specimen of interest with mature techniques, but this is not always easy. Investigating corresponding sample regions using different imaging systems often times proves to be a difficult task, as identifying sample regions of interest after switching between imaging systems based on different contrast mechanisms, and working at different resolution scales is time demanding (and sometimes impossible).

In this contribution we present a correlative approach for imaging biological samples which alleviates some of the above mentioned difficulties. It relies on a homemade multimodal setup that incorporates s-SNOM and CLSM; in this configuration the two techniques/workmodes can be operated consecutively or simultaneously to image co-localized sample regions. The proposed method is demonstrated on zebrafish retinal tissue. To the best of our knowledge no similar approaches for imaging biological specimens have been reported to date.

2. Optical setup

A diagram of the homemade multimodal system capable of in-tandem far-field ↔ near-field imaging is presented in Fig. 1. The system is based on a "sandwich" type architecture, and consists in two interlinked imaging modules that can probe overlapping field of views of a specimen positioned in-between. The upper module consists in an ASNOM system which has been previously homebuilt as an upgrade to a commercial Atomic Force Microscope (Q-scope 350, Quesant, USA). In the current configuration, for laser beam ↔ scanning probe alignment reasons, the xy probe scanning system of the Q-scope 350 has been replaced by an xy sample scanning system consisting in a piezoceramic stage MCLS03113 (MadCityLabs, USA). In the presented experiment the ASNOM module has been configured to perform imaging in the s-SNOM workmode, in a pseudoheterodyne detection scheme [22]. In this detection strategy the optical signals of interest are extracted from the intense background light using a lock-in amplifier SR844 RF (Stanford Research Systems, USA), locked on successive harmonics of the pseudoheterodyned signal [23], see Fig. 1. The bottom module of the developed system consists in a commercial inverted CLSM system (C2 + on Eclipse Ti-E, Nikon, Japan), which has been custom modified to accommodate the overlay of the ASNOM module in conditions of mechanical stability. Moreover, the Nikon C2 + CLSM has been modified so as to allow imaging sample regions that include the field of view of the ASNOM module, hence corresponding specimen areas can be imaged with both techniques without sample repositioning requirements (resulting in co-localized images).

For s-SNOM excitation we used a 638nm semiconductor laser (Omicron, Germany), with 60 μW power (measured after the objective); the focal spot of the circularly polarized beam was aligned with the position of the probe through a long working distance objective (50x, 0.42 N.A.). The NSC19/Ti-Pt probe (MikroMasch AFM probes - www.spmtips.com) has a radius of curvature in the tip's apex <35 nm, a tip height of 20-25 μm and full tip cone angle <30°. In the case of s-SNOM the tip's radius of curvature dictates the maximal attainable resolution on the xy-plane. For the CLSM investigations conducted in fluorescence we used three Nikon C2 proprietary laser lines: 405nm, 488nm, 561nm. The s-SNOM images were collected at a digital resolution of 500 × 500 pixels, and the CLSM images at 1024x1024 pixels. An earlier version of this multimodal system has been previously used for combined imaging of nanostructured polyelectrolyte capsules [14], and the home-made ASNOM

Biomedical Optics EXPRESS

module was used by itself in various experiments, e.g. mapping the dielectric function of patterned Si/SiO2 samples [15]. This imaging platform has a flexible architecture and can be easily modified so as to incorporate additional LSM and ASNOM workmodes such as multiphoton microscopy, second harmonic generation SNOM [24] or tip-enhanced fluorescence [25, 26] (providing femtosecond laser lines and appropriate detectors are available).

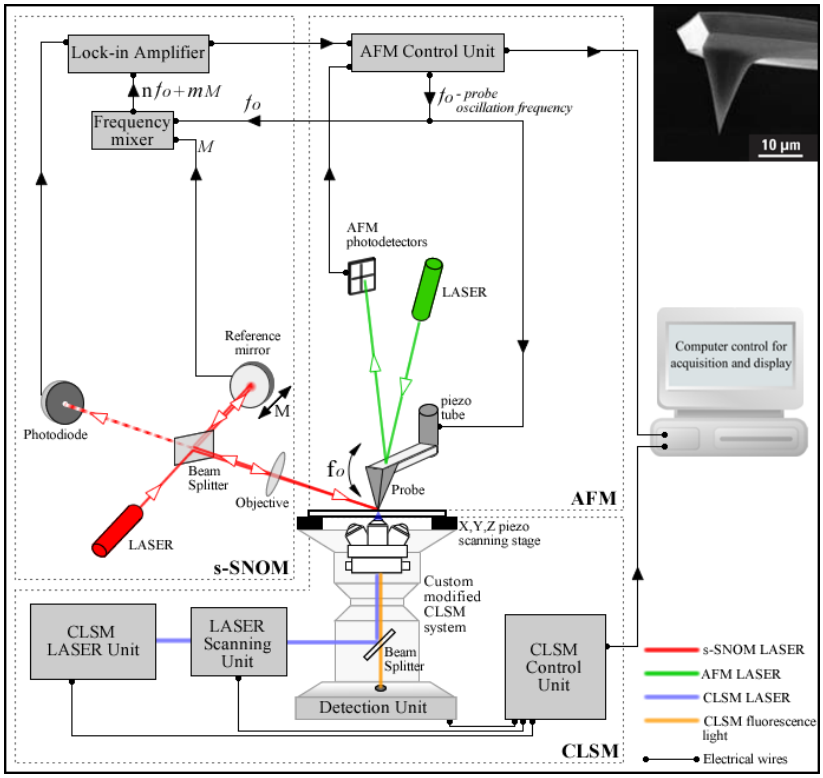

Fig. 1. Multimodal system for combined far-field ↔ near-field imaging. The home-made module positioned above the sample plane is used for s-SNOM imaging, and consists in a Michelson interferometer with the laser beam from one interferometer arm focused onto the tip apex and the other one reflected off a harmonic oscillating reference mirror. The reference beam interferes with the scattered light originated from the near-field of the sample and the interference signal contains the near-field optical information at frequencies n·fo ± m·M, where f_o is the tip's oscillation frequency, M is the mirror oscillation frequency and n, m are integers. The s-SNOM signal is collected using a lock-in amplifier locked at the n·fo ± m·M spectral harmonics. Top-righ inset: Scanning Electron Microscopy image of the NSC19/Ti-Pt probe (image courtesy of MikroMasch® AFM probes - www.spmtips.com). The imaging module positioned below the sample plane is used for CLSM imaging and consists in a custom modified commercial system.

3. Sample preparation

Two main conditions need to be satisfied for ensuring optimal imaging with the presented s-SNOM – CLSM multimodal configuration: (i) substrate & sample transparency, so that the same regions of the sample can be imaged with both techniques, (ii) reduced surface roughness of the sample region imaged with s-SNOM, as high surface roughness can translate to piezoceramic feedback inconsistencies and hence bias s-SNOM acquisition. To satisfy these two conditions we have used ultra-thin tissue sections prepared according to a recently proposed method for Correlative Light Electron Microscopy (CLEM) [27, 28]. Pieces of zebrafish retina were mounted on "cryo-pins" (Baltic Präparation, Germany #16701950),

Biomedical Optics EXPRESS

frozen in liquid nitrogen and transferred to a Ultracut EM FC6 cryo-ultramicrotome (Leica Microsystems, Germany). Further on, 100 nm thin sections were cut with a cryo-immuno diamond knife (Diatome) and then collected and deposited on 12 × 12 mm cover slips by using a "Perfect loop" (Diatome) with 2% methylcellulose (M-6385; Sigma) and 2.3 M sucrose (1:1). Using a coverslip as substrate ensures both high-transparency and minimal substrate induced roughness. The sections were subsequently processed for immunofluorescence staining with DAPI, Tom20 and BODIPY, and following this step a short postfixation with glutaraldehyde was performed. Further on, in order to protect the tissue from drying artefacts and to avoids the need of using solvents and resin embedding, which can contribute to tissue shrinkage and resin induced roughness, centrifugation was applied for covering the ultrathin Tokuyasu section with a thin layer of dried methylcellulose.

4. Results and discussion

The main aim of our work was to implement a proof-of-concept experiment that demonstrates correlative optical imaging of biological tissues with s-SNOM and CLSM used in tandem in a multimodal setup. The key advantages of this approach are: (i) availability of complementary information categories associated to the s-SNOM (label-free) and CLSM (label-based) contrast mechanisms, and (ii) availability of micro- and nanoscale optical data, which allows the observation of ultrastructural features, and their integration in a well understood context of anatomical relevance.

In Fig. 2 we present a set of s-SNOM and CLSM images collected on zebrafish retina sections. The retina lies at the back of the eye, capturing light and transmitting electrical impulses to the visual cortex in the brain via the optic nerve. The reasons behind using this sample type relates to its significance for understanding retinal regeneration mechanisms. The fish and mammalian retina are composed of similar cell types with conserved function, but unlike mammals, the zebrafish exhibit an outstanding capability to regenerate all retinal cell types, and can revert from a blind state to a state of functional vision in a matter of days. Understanding in better detail the underlying mechanisms of this capacity is of utmost importance for developing novel strategies that may stimulate similar processes in mammals [29].

CLSM and s-SNOM investigations were performed on overlapping sample regions without having to reposition the specimen, as a result of the presented architecture. The multimodal system can perform s-SNOM and CLSM imaging in consecutive or simultaneous sessions; in the case of our experiment CLSM imaging has been performed prior to s-SNOM imaging, in order to localize the sample regions of interest and to avoid contributions of the ASNOM excitation line to the CLSM channel collecting BODIPY fluorescence, due to spectral overlap. In the CLSM micrographs we can observe different layers of the retina via the fluorescent signals originating from the three dyes. Nuclei of the photoreceptor cells and of the bipolar cells are marked with DAPI (blue). The mitochondria of the photoreceptors, which are responsible for respiration and energy production, are positioned in the inner segment of the photoreceptor, near the border with the outer segment. In our CLSM micrographs, these can be observed in green, as a result of the Tom20 staining of the outer mitochondrial membrane. The outer segments, marked with BODIPY (red) – which attaches to all membrane-enclosed compartments including membrane stacks, represent the part of the photoreceptors that absorb light. In between the outer segments, infiltrations of the retinal pigment epithelium (RPE), a.k.a pigmented layer of the retina, are present. s-SNOM imaging based on amplitude and phase-contrast was performed in these areas where the RPE and outer segments co-exist in the purpose of imaging the unlabeled melanin granules of the RPE. These can be easily observed in the s-SNOM amplitude and phase images presented in Fig. 2 at optical resolutions not available in CLSM. In the employed illumination setup, melanin granules in the RPE exhibit prominent s-SNOM contrast because the excitation wavelength (638nm) is contained in the absorption band of melanin [30]. The importance of imaging

Biomedical Optics EXPRESS

melanin granules at nanoscale resolutions can be perceived through the prism of the wide number of roles that melanin plays in ocular physiology/pathology of both fish and mammals [31]. For example the melanin in the RPE acts as a free radical sink and diminishes cytotoxic lipid peroxidation, the process under which the oxidants (such as free radicals) attack the lipids containing carbon-carbon double bond(s). Melanin is also responsible for protecting the cells from (i) damage caused by oxidative stress, (ii) light toxicity and (iii) cytotoxic effects caused by ocular inflammation. It additionally plays an important role in regard to storing and releasing zinc molecules when required, which has a significant importance as various enzymes, require zinc for activation [32].

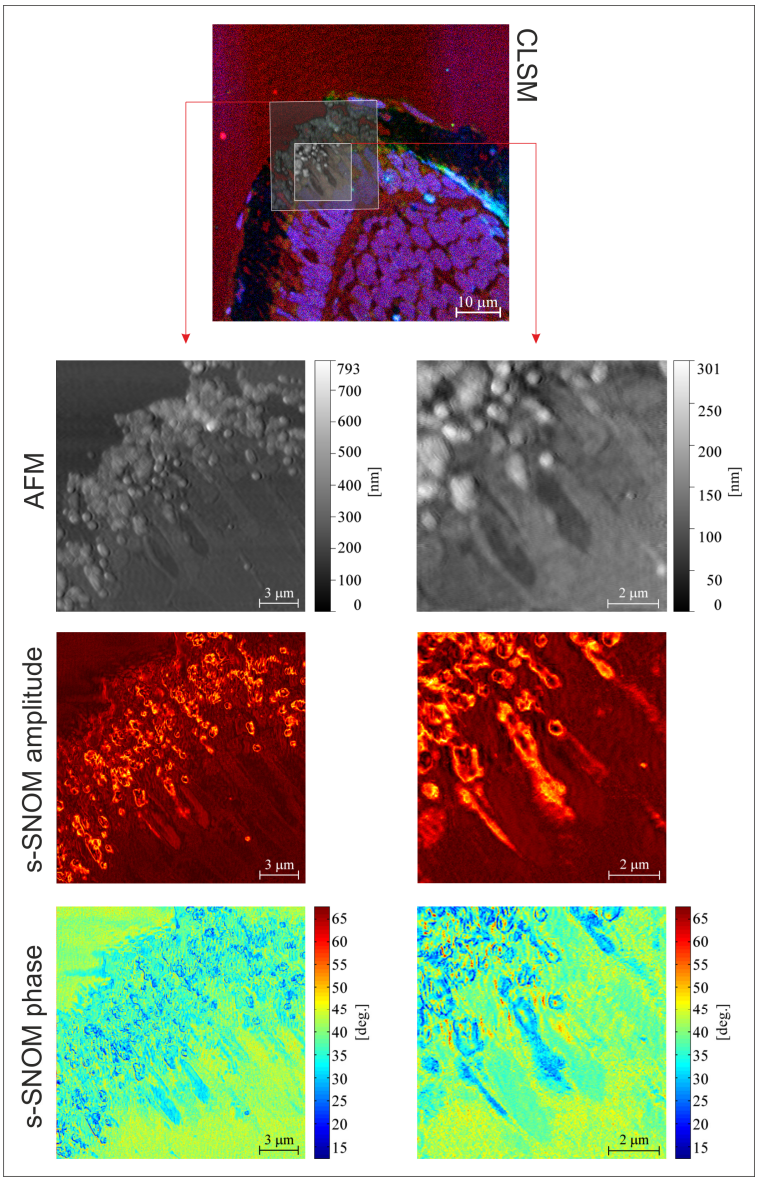

Fig. 2. Zebrafish retina investigated by CLSM, AFM and s-SNOM. To facilitate the localization of the regions imaged with AFM/s-SNOM, the AFM images are overlaid on the CLSM micrograph.

Biomedical Optics EXPRESS

In the collected s-SNOM amplitude and phase images optical signal variations can be perceived across the surface of the imaged melanin granules. These variations can be exploited for quantitatively assessing variations in the dielectric function [15], and hence optical parameters such as refractive index [33], transmittance, absorption, etc., which are important for practical applications requiring the prediction of light transport through pigmented tissue [34]. s-SNOM images based on amplitude and phase contrast are correlated but contain nonetheless complementary information [12] and simultaneous mapping of amplitude and phase of the near-field scattered light can be exploited to obtain both real and imaginary parts of the refractive index or the dielectric permittivity [15, 33]. Furthermore, s-SNOM phase images are less prone to "edge darkening" artifacts which can occur in s-SNOM amplitude images at the locations of sharp topographical steps where weaker scattering is exhibited as a result of increased distance between the tip and the sample [35].

A second set of samples was assembled using the same preparation procedure, followed by an additional step consisting in shadowing the methylcellulose layer with platinum/carbon. The last step is not necessary for neither ASNOM nor CLSM imaging, however it has a significant importance for Scanning Electron Microscopy where it allows probing topographic contrast via the detection of secondary electrons [27]. The reason for applying this shadowing procedure was to investigate whether the Pt/C layer deposited on the sample surface obstructs the detection of near-field signals originating from the retinal tissue with s-SNOM. Although s-SNOM is typically considered to be a surface characterization technique, sub-surface features can also be observed depending on their depth and the composition of superior layers [36, 37]. In the case of our experiment, the s-SNOM signals originating from the melanin granules where slightly diminished in the case of the Pt/C shadowed sample, but not enough to obstruct the observation of the structures of interest, Fig. 3. Attenuation of s-SNOM signals with depth has been thoroughly discussed to date [36–38]. At the same time, in this second set of samples the intensity of the fluorescence signals collected by CLSM was slightly enhanced as a result of fluorescence mirroring from the Pt/C layer, which relies on similar mechanisms as those exploited for fluorescence enhancement with metal-coated slides [39]. This part of our experiment indicates that samples prepared for CLEM using the method described in [27] can also be optimally imaged with the proposed approach for correlative imaging in the far-field and near-field regimes supposing a transparent substrate is used.

We consider the proposed correlative imaging approach based on CLSM and s-SNOM to be particularly useful for placing s-SNOM data into a well understood context of anatomical relevance, provided by CLSM imaging of cellular/tisullar components specifically labeled in this regard. In this scenario problems may arise when the optical properties (e.g. absorption band) of the endogenous s-SNOM contrast sources overlap with those of the contrast agents used for ensuring anatomical context availability via CLSM. To avoid such problems, careful selection of the contrast agents used for CLSM imaging depending on the optical properties of s-SNOM features of interest, and s-SNOM illumination wavelengths, is required. Furthermore, the proposed approach for correlative imaging of biological tissues with ASNOM and LSM techniques can also be adapted to be used in association with unlabeled specimens, which could represent a viable alternative to avoid undesired contributions of exogenous agents in the collected s-SNOM data sets. In correlative imaging scenarios focused on unlabeled tissue specimens, the employed LSM technique(s) needs to exploit endogenous sources of contrast, instead of exogenous contrast agents. In this regard, in a set of future experiments we plan to replace CLSM with MPM and use Two-Photon Excitation Fluorescence (TPEF) and Second Harmonic Generation (SHG) in combination with s-SNOM to image unlabeled ocular and epithelial tissues. The three techniques have a complementary usefulness in imaging non-labeled biological specimens: (i) TPEF can be used to probe the autofluorescence generated by endogenous chromophores, such as the enzyme cofactors nicotinamide adenine dinucleotide or flavin adenine dinucleotide, (ii) SHG can collect optical signals generated from non-centrosymetric molecules present in animal tissues, such as

Biomedical Optics EXPRESS

myosin, tubulin or collagen, while (iii) s-SNOM can provide valuable information based on dielectric contrast, and can quantitatively assess optical properties such as refractive index, absorption, etc [15, 33].

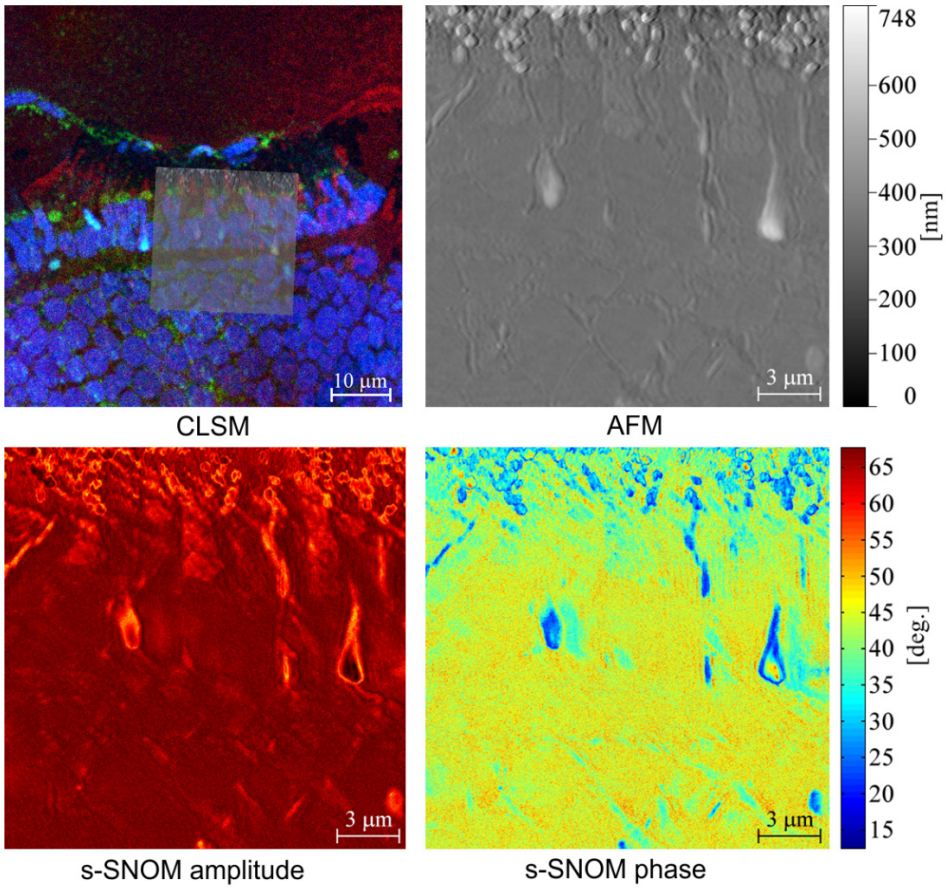

Fig. 3. Pt/C shadowed zebrafish retina investigated by CLSM, AFM and s-SNOM. To facilitate the localization of the regions imaged with AFM/s-SNOM, the AFM image is overlaid on the CLSM micrograph.

5. Conclusions

In this experiment we have demonstrated the concept of correlative imaging of biological tissues using a multimodal system incorporating CLSM and s-SNOM. In order to fulfill the conditions required for this approach, we have resorted to a sample preparation strategy previously developed for CLEM, which results in low surface roughness, high-transparency and sample robustness. Based on the proprietary label-free contrast mechanisms of s-SNOM melanin granules were observed in regions of the pigmented layer of the retina infiltrated in between the outer segments of the photoreceptor units of the retina. The evaluation of the RPE represents a topic of high interest, since its composition and function have deep implications for photoreceptor degeneration [31, 40]. CLSM was used to image stained layers of the investigated zebrafish retina, and to place s-SNOM information into a well understood anatomical context. Analogous approaches could be used for the characterization of other tissue categories such as epithelial, connective or muscular tissues, with various combinations of LSM and ASNOM variants

Biomedical Optics EXPRESS

Funding

Romanian Executive Agency for Higher Education, Research, Development and Innovation Funding (UEFISCDI) (PN-II-RU-TE-2014-4-1803 MICRONANO; PN-III-P2-2.1-PED-2016-0450 Q-NANOBIOTIC).

Acknowledgments

The authors gratefully acknowledge Dr. José María Mateos and Dr. Urs Ziegler at the Center for Microscopy and Image Analysis, University of Zurich for their thoughtful explanations over the CLEM tissue preparation method and for preparing the samples, and to Dr. Ruxandra Bachmann-Gagescu and Prof. Stephan Neuhauss at the Institute for Molecular Life Sciences, University of Zurich for providing the zebra fish retina fragments.

Disclosures

The authors declare that there are no conflicts of interest related to this article.